

Is the large-scale structure traced by the BOSS LOWZ galaxies consistent with *Planck*?

ZHIWEI SHAO ¹, YING ZU ^{1,2} AND HUANYUAN SHAN ^{3,4}

¹*Department of Astronomy, School of Physics and Astronomy, and Shanghai Key Laboratory for Particle Physics and Cosmology, Shanghai Jiao Tong University, Shanghai 200240, China; yingzu@sjtu.edu.cn*

²*Key Laboratory for Particle Physics, Astrophysics and Cosmology, Ministry of Education, Shanghai Jiao Tong University, Shanghai 200240, China*

³*Shanghai Astronomical Observatory (SHAO), Nandan Road 80, Shanghai 200030, China*

⁴*University of Chinese Academy of Sciences, Beijing 100049, China*

ABSTRACT

Recently, several studies reported a significant discrepancy between the clustering and lensing of the Baryon Oscillation Spectroscopic Survey (BOSS) galaxies in the *Planck* cosmology. We construct a simple yet powerful model based on the linear theory to assess whether this discrepancy points toward deviations from *Planck*. Focusing on scales $10 < R < 30 h^{-1} \text{Mpc}$, we model the amplitudes of clustering and lensing of BOSS LOWZ galaxies using three parameters: galaxy bias b_g , galaxy-matter cross-correlation coefficient r_{gm} , and A , defined as the ratio between the true and *Planck* values of σ_8 . Using the cross-correlation matrix as a diagnostic, we detect systematic uncertainties that drive spurious correlations among the low-mass galaxies. After building a clean LOWZ sample with $r_{gm} \sim 1$, we derive a joint constraint of b_g and A from clustering+lensing, yielding $b_g = 2.47^{+0.36}_{-0.30}$ and $A = 0.81^{+0.10}_{-0.09}$, i.e., a 2σ tension with *Planck*. However, due to the strong degeneracy between b_g and A , systematic uncertainties in b_g could masquerade as a tension with $A=1$. To ascertain this possibility, we develop a new method to measure b_g from the cluster-galaxy cross-correlation and cluster weak lensing using an overlapping cluster sample. By applying the independent bias measurement ($b_g = 1.76 \pm 0.22$) as a prior, we successfully break the degeneracy and derive stringent constraints of $b_g = 2.02^{+0.16}_{-0.15}$ and $A = 0.96 \pm 0.07$. Therefore, our result suggests that the large-scale clustering and lensing of LOWZ galaxies are consistent with *Planck*, while the different bias estimates may be related to some observational systematics in the target selection.

Keywords: cosmological parameters — cosmology: observations — cosmology: theory — dark matter — gravitational lensing: weak — large-scale structure of universe

1. INTRODUCTION

Anchored by the latest *Planck* observations of the cosmic microwave background (CMB) anisotropies at recombination (Planck Collaboration et al. 2020), the standard Λ CDM cosmological model under General Relativity (GR) provides a remarkably good description of the evolution of our Universe toward later epochs, including the expansion history measured by baryon acoustic oscillations (Alam et al. 2021) and Type Ia supernovae (Scolnic et al. 2018) as well as the growth history measured by redshift space distortion, cosmic shear, and galaxy clusters (see Weinberg et al. 2013, for an extensive review). However, tensions may still arise when one compares low-redshift measurements of the matter density Ω_m and the present-day amplitude of matter clustering, characterized by σ_8 , the rms matter fluctuation in $8 h^{-1} \text{Mpc}$ spheres, to the values expected from extrapolating CMB anisotropies forward from recombination to $z=0$, e.g., $\Omega_m^{\text{CMB}} = 0.3153$ and $\sigma_8^{\text{CMB}} = 0.8111$ using *Planck*.

Most notably, recent cosmic shear studies found a $1-3\sigma$ lower value (Asgari et al. 2021; Secco et al. 2022; Amon et al. 2022; Huterer 2022) of the parameter combination $S_8 \equiv \sigma_8 (\Omega_m / 0.3)^{0.5}$ compared to *Planck* (but see Amon & Efstathiou 2022, for a plausible non-linear solution). An alternative manifestation of this S_8 -tension is the apparent mismatch between the clustering and galaxy-galaxy (g-g) lensing of the Baryon Oscillation Spectroscopic Survey (BOSS) galaxies when assuming *Planck* cosmology (a.k.a., lensing-is-low; Leauthaud et al. 2017; Lange et al. 2019). In this letter, we examine the consistency (or lack thereof) between σ_8^{CMB} and the σ_8 measured from the clustering and g-g lensing of BOSS LOWZ galaxies over scales between 10 and $30 h^{-1} \text{Mpc}$. In particular, we elucidate the role of the galaxy bias b_g in this consistency test by introducing an independent prior on b_g , measured with the help of an overlapping sample of clusters.

Although the existence of a lensing-is-low effect on scales below $\sim 5 h^{-1} \text{Mpc}$ remains a subject of intense debate (More

et al. 2015; Yuan et al. 2020; Lange et al. 2021; Chaves-Montero et al. 2022; Contreras et al. 2022), using data from three different lensing surveys Amon et al. (2023) demonstrated that on scales above $5.25 h^{-1}\text{Mpc}$, there exists a 2.3σ discrepancy between clustering and g-g lensing in the *Planck* cosmology for the entire BOSS sample ($\sim 1.5\sigma$ for the LOWZ galaxies between $0.15 < z < 0.31$). Compared with the lensing-is-low effect on small scales, the large-scale discrepancy is a more “direct” tension with *Planck* — it does not depend on the complex modelling of galaxy-halo connection, which on small scales is plagued by galaxy assembly bias and baryonic feedback (Salcedo et al. 2022; Beltz-Mohrmann et al. 2022). Therefore, it is imperative that this direct tension be assessed in a simple framework that confronts the LOWZ clustering+lensing measurements with the prediction by the *Planck* $\Lambda\text{CDM}+\text{GR}$ model at asymptotically large scales (i.e., $> 10 h^{-1}\text{Mpc}$), where structure growth follows the linear theory and galaxy bias becomes scale-independent.

On scales above $10 h^{-1}\text{Mpc}$, galaxy clustering and g-g lensing are measuring

$$\xi_{\text{gg}} = b_{\text{g}}^2 \xi_{\text{mm}} \propto b_{\text{g}}^2 \sigma_8^2 \quad (1)$$

and

$$\xi_{\text{gm}} = b_{\text{g}} r_{\text{gm}} \xi_{\text{mm}} \propto b_{\text{g}} r_{\text{gm}} \sigma_8^2, \quad (2)$$

respectively, where ξ_{mm} is the matter correlation and $r_{\text{gm}} \rightarrow 1$ is the cross-correlation coefficient between galaxies and matter (Cacciato et al. 2012). Note that we fix the value of Ω_{m} to be $\Omega_{\text{m}}^{\text{CMB}}$, so that the S_8 -tension simplifies into a σ_8 -tension. A joint analysis of clustering and g-g lensing can then measure

$$\xi_{\text{gm}} / \sqrt{\xi_{\text{gg}}} = r_{\text{gm}} \sigma_8 \rightarrow \sigma_8, \quad (3)$$

thereby cancelling the unknown¹ nuisance parameter b_{g} . Thus, a strong discrepancy between clustering and g-g lensing in *Planck* is usually interpreted as the evidence of the ratio

$$A \equiv \sigma_8 / \sigma_8^{\text{CMB}}, \quad (4)$$

significantly deviating from unity (e.g., $A < 1$ means lensing-is-low). For instance, Wibking et al. (2020) constructed a Halo Occupation Distribution-based nonlinear emulator to constrain cosmology from jointly modelling the clustering and g-g lensing of the LOWZ galaxies on scales above $0.6 h^{-1}\text{Mpc}$, finding a 3.5σ (2.6σ if limited to $> 2 h^{-1}\text{Mpc}$) evidence of $A < 1$. By explicitly modelling g-g lensing in the form of $\Omega_{\text{m}} r_{\text{gm}} \sqrt{\xi_{\text{mm}} \xi_{\text{gg}}}$, Singh et al. (2020) found a similar $\sim 3\sigma$ discrepancy with *Planck* for a minimum scale of $2 h^{-1}\text{Mpc}$ using the LOWZ galaxies. They also

found the discrepancy persists at the level of $\sim 1.5\sigma$ when limited to scales $> 10 h^{-1}\text{Mpc}$.

Alternatively, a clustering-lensing mismatch could be the result of having systematic errors that drive r_{gm} below unity or/and an incorrect clustering amplitude, leading to an imperfect cancellation of b_{g} in Equation 3. Although both possibilities are generally considered unlikely for well-defined galaxy samples and are thus omitted in previous studies, Zu (2020) found that the clustering of LOWZ galaxies on scales above $10 h^{-1}\text{Mpc}$ exhibits a non-monotonic trend with stellar mass M_* , with the low- M_* bin having a higher clustering amplitude than the intermediate- M_* one. Zu (2020) interpreted this clustering anomaly as the evidence for the low- M_* galaxies being the satellites of massive haloes. In this letter, we demonstrate that the clustering anomaly is instead caused by some unknown systematic uncertainties associated with the BOSS LOWZ sample, probably due to the complex target selection criteria of BOSS galaxies (Reid et al. 2016).

After building a clean sample of LOWZ galaxies free of the clustering anomaly in §2, we reproduce the lensing-is-low effect using our linear framework in §3. After developing a novel method of measuring b_{g} from an overlapping sample of galaxy clusters, we demonstrate in §4 that by applying this measurement as a prior on b_{g} , we can mitigate the impact of systematic uncertainties in b_{g} and resolve the direct tension between σ_8 and σ_8^{CMB} originated from the large scales. We summarize our results and look to the future in §5.

2. A “CLEAN” SAMPLE OF LOWZ GALAXIES

2.1. The BOSS LOWZ galaxies

As part of the SDSS-III programme (Eisenstein et al. 2011), BOSS (Dawson et al. 2013) observed the spectra of 1.5 million galaxies over a sky area of $\sim 10000 \text{ deg}^2$ at $0.15 < z < 0.7$. The BOSS targets were selected from the Data Release 8 (DR8; Aihara et al. 2011) of SDSS five-band imaging, using two separate sets of colour and magnitude cuts for the LOWZ ($0.15 < z < 0.43$) and CMASS ($0.43 < z < 0.7$) samples (Reid et al. 2016). We use the DR12 of the BOSS LOWZ sample (Alam et al. 2015) and limit our analysis to the Northern Galactic Cap. We adopt the aperture-corrected stellar mass measurements by Chen et al. (2012), but reduce the stellar mass values by 0.155 dex to be consistent with the SDSS main galaxies at $z < 0.1$ (Guo et al. 2018).

In this letter, we focus on the LOWZ galaxies in the redshift range $z = [0.2, 0.3]$, for which we have a volume-complete sample of photometric clusters with excellent photo- z accuracy in the same footprint from redMaPPer (Rykoff et al. 2014). We use 4580 clusters with richness λ above 20 from the SDSS redMaPPer v6.3 catalogue (Rykoff et al. 2016). Our results do not change when using a higher threshold of $\lambda = 30$ or only clusters with spectroscopic redshifts. As will be demonstrated later in §4, this

¹ The cancellation, however, requires $b_{\text{g}} = \xi_{\text{gm}} / \xi_{\text{gg}}$, which puts a constraint on the galaxy-halo connection if the small scales are included.

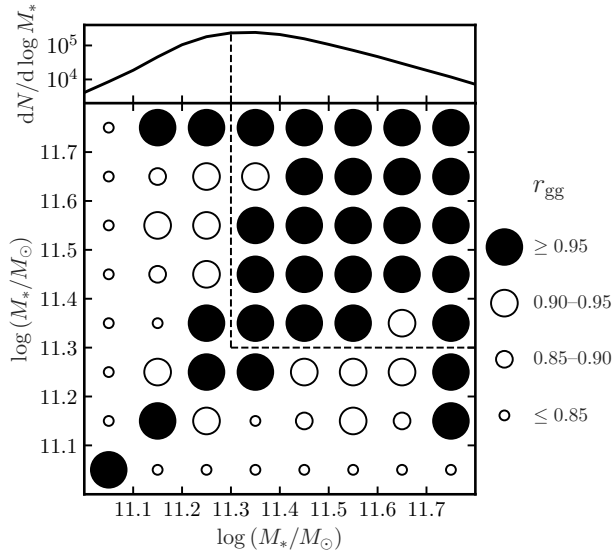


Figure 1. Cross-correlation matrix \mathcal{Q} . The size of each circle corresponds to the value of the cross-correlation coefficient r_{gg} between two stellar mass bins, indicated by the four circles on the right. Filled circles represent near-perfect correlations with $r_{\text{gg}} \geq 0.95$. The black solid curve on top shows the stellar mass distribution of the LOWZ galaxies, with the black dashed line indicating the stellar mass limit ($\log M_* = 11.3$) of our C-LOWZ sample selection.

overlapping cluster sample allows us the unique opportunity to make an independent measurement of b_{g} , without resorting to galaxy clustering or g-g lensing.

2.2. Selecting a clean sample of LOWZ galaxies

Ideally, we hope to select a “clean” LOWZ sample that has $r_{\text{gm}} = 1$ on scales above $10 h^{-1} \text{Mpc}$, but r_{gm} is not directly accessible. Following an indirect diagnostic proposed by Tegmark & Bromley (1999), we divide the overall LOWZ galaxy sample into eight narrow bins by stellar mass ($\Delta \log M_* = 0.1$ dex), and then compute the galaxy-galaxy cross-correlation coefficient r_{gg}^{ij} between each pair combination (i, j), yielding an 8×8 cross-correlation matrix $\mathcal{Q} \equiv [r_{\text{gg}}^{ij}]$. We search \mathcal{Q} for a contiguous block within which the average r_{gg} is close to unity, and identify the stellar mass range of that block as a *clean* sample. The rationale is as follows. If the i -th and j -th bins are both perfectly correlated with matter, then they must also be perfectly correlated with each other (i.e., $r_{\text{gg}}^{ij} = 1$). Conversely, if we find imperfect correlations between the two, then $r_{\text{gm}} < 1$ must be true for at least one of the two bins. Therefore, by culling the $r_{\text{gg}} < 1$ regions from \mathcal{Q} , we remove the $r_{\text{gm}} < 1$ galaxies that are potentially subjected to observational systematics.

We compute r_{gg}^{ij} as

$$r_{\text{gg}}^{ij} = \frac{w_p^{ij}}{\sqrt{w_p^{ii} w_p^{jj}}} \Big|_{10 < R < 30}, \quad (5)$$

where w_p^{ii} and w_p^{jj} are the projected auto-correlation functions of the i -th and j -th bins, respectively, and w_p^{ij} is the projected cross-correlation function between the two bins, all evaluated over the projected separation of $R \in [10, 30] h^{-1} \text{Mpc}$. We compute the projected correlation functions $w_p(R)$ by integrating the 2D redshift-space correlation function $\xi^{rs}(R, \Pi)$ along the line-of-sight distance Π

$$w_p(R) = \int_{-\Pi_{\text{max}}}^{+\Pi_{\text{max}}} \xi^{rs}(R, \Pi) d\Pi, \quad (6)$$

where we set the integration limit Π_{max} to $50 h^{-1} \text{Mpc}$. For measuring $\xi^{rs}(R, \Pi)$, we use the Landy-Szalay estimator (Landy & Szalay 1993) and estimate the associated uncertainty matrix by applying the jackknife re-sampling method over 128 sub-divided regions across the footprint.

Figure 1 visualizes the correlation matrix \mathcal{Q} , with the size of each circle at column i and row j representing the value of r_{gg}^{ij} , which we classify into four categories listed on the right. Surprisingly, almost all of the matrix elements that involve bins with $\log M_* < 11.3$ are below 0.95, hinting at the existence of unknown systematics among the low- M_* galaxies. The highest- r_{gg} category ($r_{\text{gg}} > 0.95$) is highlighted by the filled circles, which are mostly enclosed within the dashed lines, i.e., $\log M_* \geq 11.3$. The dashed line also coincides with the peak of the stellar mass distribution of the LOWZ sample (top), suggesting that the unknown systematics are likely from the target selection in the low-mass range with high incompleteness. In particular, we detect significant spurious correlations over large line-of-sight distances within the galaxies with $\log M_* < 11.3$, which explains the aforementioned clustering anomaly found in Zu (2020).

Informed by the \mathcal{Q} diagnostics, we select LOWZ galaxies with $\log M_* \geq 11.3$ into our “clean” LOWZ sample (hereafter referred to as C-LOWZ), and use the C-LOWZ sample for all subsequent analyses in this letter.

2.3. Clustering and weak lensing measurements

We make use of the projected auto-correlations of C-LOWZ galaxies ($w_{p,\text{gg}}$) and redMaPPer clusters ($w_{p,\text{cc}}$), as well as the cross-correlation between the two ($w_{p,\text{cg}}$) in our analyses. The three correlation functions $w_p(R)$ are measured in the same way as described by Equation 6. For the weak lensing by C-LOWZ galaxies and redMaPPer clusters, we measure the surface density contrast profile $\Delta\Sigma(R)$ using the shear catalogue derived from the Dark Energy Camera Legacy Survey (DECaLS; Dey et al. 2019). The same DECaLS data were used in the fiducial cluster weak lensing study of Zu et al. (2021), who found excellent agreement between the $\Delta\Sigma$ measured from DECaLS and that from SDSS imaging using the re-Gaussianization algorithm (Reyes et al. 2012), but the uncertainties in the DECaLS measurements are smaller by roughly a factor of two thanks to the deeper

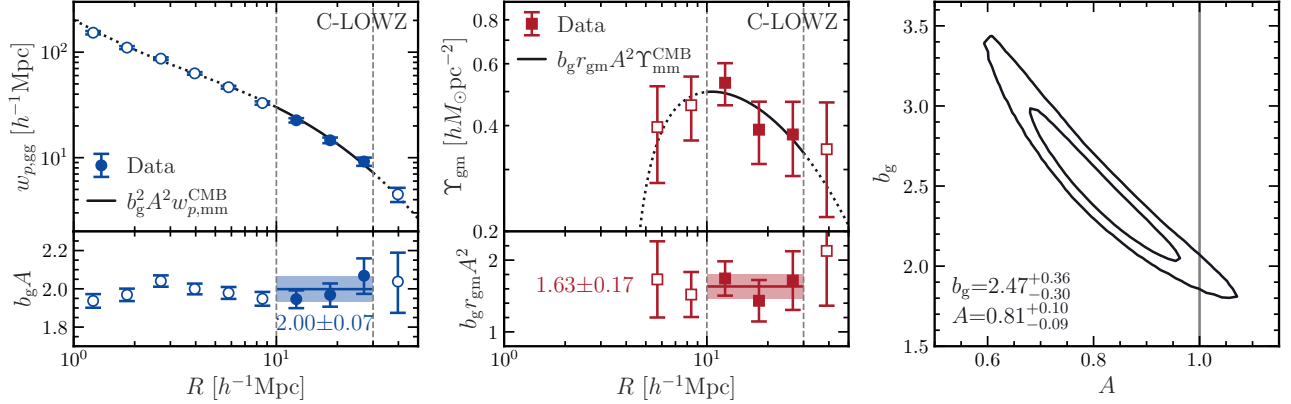


Figure 2. *Left:* Comparison of the projected clustering of C-LOWZ galaxies between the measurements (circles with errorbars) and the best-fitting linear model prediction (solid curve) on scales $10 < R < 30 h^{-1} \text{Mpc}$ (within the vertical dashed lines). The constraint on the product of $b_g A$ is shown by the horizontal band in the bottom panel. *Middle:* Similar to the left panel, but for the g-g lensing signal Υ_{gm} . *Right:* Joint posterior distribution of b_g and A derived from combining the clustering and g-g lensing of C-LOWZ galaxies. Contours indicate the 68% and 95% 2D confidence regions, with the marginalized 1σ constraints listed in the bottom left.

depth. Note that the SDSS g-g lensing measurements were used by Wibking et al. (2020), Singh et al. (2020), and Lange et al. (2021) in their LOWZ analyses.

Unlike $w_p(R)$, the $\Delta\Sigma(R)$ signal on scales above $10 h^{-1} \text{Mpc}$ is contaminated by the non-linear structure growth below $10 h^{-1} \text{Mpc}$ (Zu & Mandelbaum 2015). To remedy this, we measure the annular differential surface density (ADSD) Υ , defined as

$$\Upsilon(R) = \Delta\Sigma(R) - \left(\frac{R_0}{R}\right)^2 \Delta\Sigma(R_0), \quad (7)$$

where we set the minimum scale $R_0 = 4 h^{-1} \text{Mpc}$. Originally proposed by Baldauf et al. (2010), Υ removes all the information from scales below R_0 and thus can be safely predicted using the linear theory. Following Mandelbaum et al. (2013), we interpolate the value of $\Delta\Sigma(R_0)$ using the best-fitting power-law that describes $\Delta\Sigma$ between $1 h^{-1} \text{Mpc}$ and $10 h^{-1} \text{Mpc}$ (also see Singh et al. 2020).

3. LINEAR ASSESSMENT METHOD

To facilitate the σ_8 -tension assessment on linear scales, we follow the practice of Zu et al. (2014) and keep the shape of the linear matter power spectrum $P_{\text{lin}}(k)$ fixed to that of *Planck* $P_{\text{lin}}^{\text{CMB}}(k)$. With a fixed $P_{\text{lin}}(k)$ shape, a single value of A specifies the full matter correlation function ξ_{mm} via

$$\xi_{\text{mm}}(r) = A^2 \xi_{\text{mm}}^{\text{CMB}}(r). \quad (8)$$

where $\xi_{\text{mm}}^{\text{CMB}}(r)$ is the nonlinear matter correlation predicted from $P_{\text{lin}}^{\text{CMB}}(k)$ using the prescription of Takahashi et al. (2012). We assume the mean redshift of C-LOWZ ($z=0.256$) for all calculations.

Focusing exclusively on scales $10 < R < 30 h^{-1} \text{Mpc}$, we model the $w_{p,\text{gg}}$ measurement as

$$w_{p,\text{gg}}(R) = b_g^2 A^2 f_{\text{rrsd}}(R | b_g) w_{p,\text{mm}}^{\text{CMB}}(R), \quad (9)$$

where $w_{p,\text{mm}}^{\text{CMB}}(R)$ is the projected matter auto-correlation

$$w_{p,\text{mm}}^{\text{CMB}}(R) = 2 \int_R^{\sqrt{\Pi_{\text{max}}^2 + R^2}} \xi_{\text{mm}}^{\text{CMB}}(r) \frac{r \, dr}{\sqrt{r^2 - R^2}}, \quad (10)$$

and $f_{\text{rrsd}}(R | b_g)$ accounts for the scale-dependent enhancement of $w_{p,\text{gg}}(R)$ due to the residual redshift-space distortion (RRSD) effect. We calculate f_{rrsd} using the modified linear Kaiser formalism of van den Bosch et al. (2013). For the C-LOWZ sample, f_{rrsd} is about 8% and 30% at $R=10$ and $30 h^{-1} \text{Mpc}$, respectively. The b_g -dependence of f_{rrsd} is very weak and does not provide any meaningful constraint on b_g . Therefore, our clustering model of Equation 9 constrains the parameter combination $b_g A$, which turns into a bias measurement $b_g^{\text{clustering}}$ for any given value of A .

By the same token, the ADSD profile Υ_{gm} can be modelled as

$$\Upsilon_{\text{gm}}(R) = b_g r_{\text{gm}} A^2 \Upsilon_{\text{mm}}^{\text{CMB}}(R), \quad (11)$$

and the matter-matter ADSD in *Planck* $\Upsilon_{\text{mm}}^{\text{CMB}}$ can be predicted from Equation 7 using $\Delta\Sigma_{\text{mm}}^{\text{CMB}}$

$$\Delta\Sigma_{\text{mm}}^{\text{CMB}}(R) = \langle \Sigma_{\text{mm}}^{\text{CMB}}(< R) \rangle - \Sigma_{\text{mm}}^{\text{CMB}}(R), \quad (12)$$

where

$$\Sigma_{\text{mm}}^{\text{CMB}}(R) = \Omega_{\text{m}}^{\text{CMB}} \rho_{\text{crit}} \int_{-\infty}^{+\infty} [1 + \xi_{\text{mm}}^{\text{CMB}}(r)] \frac{r \, dr}{\sqrt{r^2 - R^2}}, \quad (13)$$

and

$$\langle \Sigma_{\text{mm}}^{\text{CMB}}(< R) \rangle = \frac{2}{R^2} \int_0^R \Sigma_{\text{mm}}^{\text{CMB}}(R') R' \, dR'. \quad (14)$$

Similarly, our lensing model of Equation 11 constrains the parameter combination $b_g r_{\text{gm}} A^2$, which then provides a bias measurement b_g^{lensing} for any given r_{gm} at fixed A .

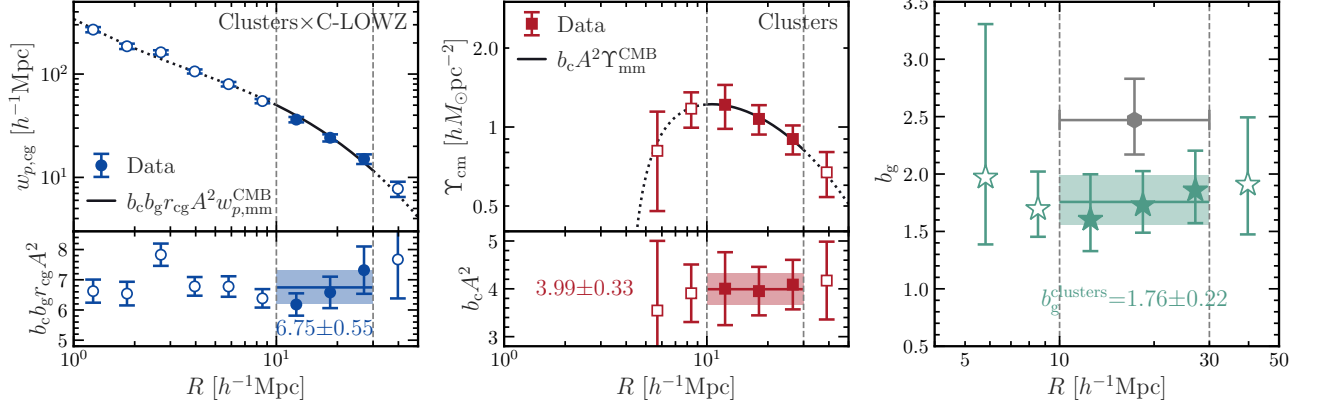


Figure 3. Cluster-based bias measurement for the C-LOWZ galaxies (right panel) from the combination of cluster-galaxy cross-correlation (left) and cluster weak lensing (middle). The formats of the left and middle panels are the same as in Figure 2. In the right panel, star symbols with errorbars represent the ratio calculated using Equation 18, from which we derive $b_g^{\text{clusters}} = 1.76 \pm 0.22$ (green horizontal band). Gray hexagon with errorbar indicates the bias constraint ($2.47^{+0.36}_{-0.30}$) from the right panel of Figure 2.

Combining the clustering model (Equation 9) and the lensing model (Equation 11), our linear assessment model has only three parameters: b_g , r_{gm} , and A . Among the three, A is our key parameter which quantifies the σ_8 -tension, b_g is our primary nuisance parameter that may still be affected by observational systematics, and r_{gm} should be close to unity for our C-LOWZ galaxy sample. We perform a suite of three Bayesian inference analyses by applying the clustering model, the lensing model, and the combined model to the measurements of $w_{p,gg}$, Υ_{gm} , and $w_{p,gg} + \Upsilon_{gm}$, respectively, of the C-LOWZ sample on scales $10 < R < 30 h^{-1} \text{Mpc}$. Assuming Gaussian likelihoods, we can derive the posterior distributions of $b_g A$, $b_g r_{gm} A^2$, and the joint distribution of b_g and A . For the joint constraint, we apply a conservative Gaussian prior on $r_{gm} \sim \mathcal{N}(1, 0.05^2)$.

Figure 2 presents the results of the clustering-only (left), lensing-only (middle), and joint (right) constraints. On the left panel, the $w_{p,gg}$ measurement (circles with errorbars) is well described by the prediction from the best-fitting clustering model (solid curve) on scales $10 < R < 30 h^{-1} \text{Mpc}$. Dotted curve segments are the extrapolation of the linear model into the nonlinear or very low signal-to-noise regimes, and should not be compared with the data (open circles). The bottom subpanel shows the square root of the ratio between the measurement and $w_{p,mm}^{\text{CMB}}$, which gives the constraint on $b_g A$ as 2.00 ± 0.07 (horizontal band). Similarly, the middle panel presents the data vs. prediction comparison in the main panel, as well as the ratio profile in the bottom sub-panel, yielding a constraint of $b_g r_{gm} A^2 = 1.63 \pm 0.17$. If assuming the *Planck* cosmology (i.e., $A=1$), we would obtain $b_g^{\text{clustering}} = 2.00 \pm 0.07$ and $b_g^{\text{lensing}} = 1.63 \pm 0.17$, reproducing a lensing-is-low effect of 2σ on large scales.

The right panel of Figure 2 shows the 2D constraint on the A vs. b_g plane after marginalizing over the uncertainties of r_{gm} . The contour lines are the 68% and 95% confidence

limits, yielding the 1D posterior constraints as $b_g = 2.47^{+0.36}_{-0.30}$ and $A = 0.81^{+0.10}_{-0.09}$. Therefore, when applied to the clustering and g-g lensing measurements on large scales, our linear assessment method detects a $\sim 2\sigma$ discrepancy with *Planck*, reproducing the S_8 -tension reported by previous studies.

However, a strong degeneracy exists between b_g and A , and the 2D constraint remains marginally consistent with *Planck* within 1.5σ . Given the presence of unknown systematics in the LOWZ sample demonstrated by Figure 1, it is plausible that other systematics of the similar origin may remain within our C-LOWZ sample in a way that affects the b_g measurement but evades our detection using the Tegmark & Bromley (1999) method. In order to break the strong degeneracy seen in the right panel of Figure 2, we need to place an external prior on b_g using an independent measurement of b_g from a different dataset than galaxy clustering and g-g lensing.

4. CLUSTER-BASED MEASUREMENT OF b_g

Adopting the same philosophy of §3, we can model the projected cluster-galaxy cross-correlation $w_{p,cg}$ as

$$w_{p,cg}(R) = b_c b_g r_{cg} A^2 f_{\text{rrsd}}(R | b_c, b_g) w_{p,mm}^{\text{CMB}}(R), \quad (15)$$

where b_c is the cluster bias, f_{rrsd} accounts for the cluster-galaxy RRSD, and r_{cg} is the cluster-galaxy cross-correlation coefficient. We can directly measure r_{cg} via

$$r_{cg} = \frac{w_{p,cg}}{\sqrt{w_{p,cc} w_{p,gg}}} \Bigg|_{10 < R < 30}, \quad (16)$$

where $w_{p,cc}$ is the projected auto-correlation of clusters. Likewise, the cluster weak lensing Υ_{cm} can be modelled as

$$\Upsilon_{cm}(R) = b_c r_{cm} A^2 \Upsilon_{mm}^{\text{CMB}}(R), \quad (17)$$

where r_{cm} is the cluster-matter cross-correlation coefficient. For the massive clusters that are robustly detected from imaging (i.e., without spectroscopic target selection), we can safely assume r_{cm} to be unity. Therefore, by combining the two measurements we can cancel b_c to obtain

$$b_g^{\text{clusters}} = \frac{1}{f_{\text{rrsd}} r_{\text{cg}}} \left(\frac{w_{p,\text{cg}}}{w_{p,\text{mm}}^{\text{CMB}}} \right) \left(\frac{\Upsilon_{\text{cm}}}{\Upsilon_{\text{mm}}^{\text{CMB}}} \right)^{-1}, \quad (18)$$

i.e., a cluster-based b_g measurement that is independent of A , galaxy clustering, and g-g lensing².

We apply the new bias measurement method to the C-LOWZ galaxies and the overlapping redMaPPer clusters, with the results shown in Figure 3. The left and middle panels illustrate the constraints from the clustering-only and lensing-only measurements, respectively, with the same format as that of Figure 2. In particular, the clustering constraint on the parameter combination $b_c b_g r_{\text{cg}} A^2$ is 6.75 ± 0.55 , and the lensing constraint is $b_c A^2 = 3.99 \pm 0.33$. With $r_{\text{cg}} = 0.96 \pm 0.03$ measured via Equation 16, we can compute b_g via Equation 18. Our new independent constraint on b_g is $b_g^{\text{clusters}} = 1.76 \pm 0.22$, indicated by the horizontal green band in the right panel of Figure 3. Compared to our previous constraint using galaxy clustering and g-g lensing (gray hexagon with errorbar), the new b_g^{clusters} measurement is significantly lower, signalling a 2σ tension in b_g .

Figure 4 compares the b_g^{clusters} measurement, which is A -independent (green band), to the clustering-only $b_g^{\text{clustering}}$ (blue circles) and lensing-only b_g^{lensing} (red squares) measurements assuming four different cosmologies. For the lensing-only measurements, we assume $r_{\text{gm}} = 1$ and 0.95 for the filled and open squares, respectively. In the case of *Planck* ($A=1$), although $b_g^{\text{clustering}}$ and b_g^{lensing} are mutually discrepant beyond 1σ , both are individually consistent with b_g^{clusters} well within 1σ . As we move away from *Planck* by decreasing A , the $b_g^{\text{clustering}}$ and b_g^{lensing} values increase by different amounts so as to become more consistent with each other, echoing the claim that a low- σ_8 cosmology could resolve the lensing-is-low tension; Meanwhile, however, both bias values become progressively more discrepant with b_g^{clusters} , which does not vary with A . Therefore, although a low- σ_8 cosmology could resolve the discrepancy between $b_g^{\text{clustering}}$ and b_g^{lensing} , it exacerbates the tension of the two biases with b_g^{clusters} .

The strong discrepancy between b_g^{clusters} and the other two biases persists when we adopt a representative low- S_8 cosmology (bottom panel) that alleviates the lensing-is-low problem, with the parameters drawn from the table 2 of Lange et al. (2019). In this case, the $P(k)$ shape is no

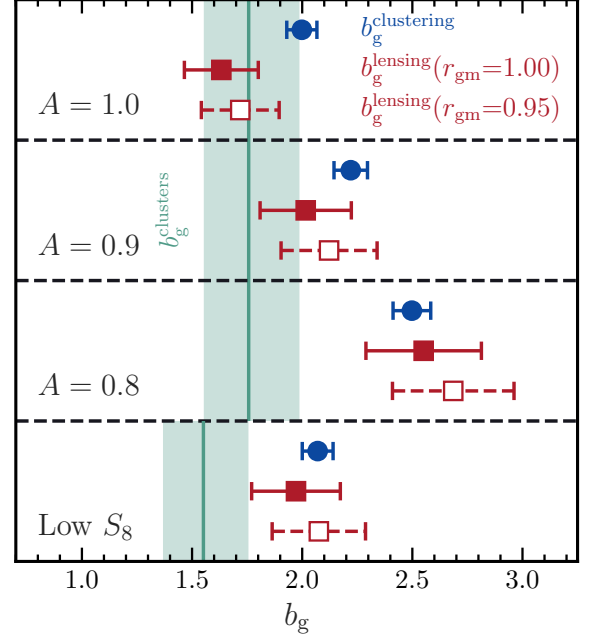


Figure 4. Comparison between galaxy biases measured from the cluster-based method (green vertical band), galaxy clustering (blue circles), and g-g lensing (red squares), under four different cosmologies, including *Planck* ($A=1.0$), two low- σ_8 cosmologies with $A=0.9$ and 0.8 , and a representative low- S_8 cosmology that resolves the clustering-lensing mismatch. Filled (open) red squares are the b_g^{lensing} estimates when assuming $r_{\text{gm}}=1$ (0.95).

longer fixed to that of *Planck* and $\Omega_{\text{m}} \neq \Omega_{\text{m}}^{\text{CMB}}$. Accordingly, the value of b_g^{clusters} shifts to 1.55 ± 0.19 , but still disagrees strongly with the clustering- and lensing-only estimates. Therefore, the existence of the b_g -tension is robust against variations in the shape of $P(k)$ or Ω_{m} .

Since the cluster-based bias measurement is independent of A and derived from external datasets, we can incorporate $b_g^{\text{clusters}} = 1.76 \pm 0.22$ as a prior in the Bayesian analysis using our linear assessment model developed in §3. Figure 5 shows the two sets of posterior constraints on the model parameters in both 1D (diagonal) and 2D (off-diagonal) parameter spaces, one with the b_g -prior on (dark filled histograms and contours) and the other off (light open). The contour levels are the 68% and 95% confidence limits, with the thin dashed curve in the bottom right panel indicating our b_g prior, while the two sets of 1σ constraints are listed on the top right. The 1D posterior distribution of r_{gm} coincides with the Gaussian prior on r_{gm} (thin dashed) when the b_g prior is off, but slides to $r_{\text{gm}} = 0.97 \pm 0.05$ when the b_g prior is on, consistent with $r_{\text{cg}} = 0.96 \pm 0.03$ and $r_{\text{cm}} = 1$. Meanwhile, our 1D posterior constraint on b_g ($2.02^{+0.16}_{-0.15}$) is significantly lower than the prior-off constraint ($2.47^{+0.36}_{-0.30}$), albeit slightly higher than the prior.

² Although the g-g and cluster lensing are measured from the same shear catalogue, the uncertainties are both dominated by the shape noise, so that the two lensing signals can be considered independent.

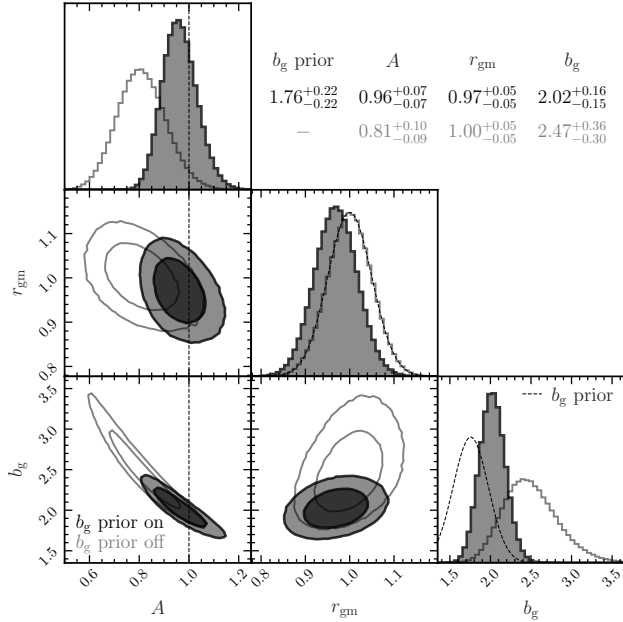


Figure 5. Constraints on the three parameters of the linear assessment model from our fiducial Bayesian analysis using the b_g prior (dark filled contours/histograms). Light open contours/histograms show the constraints from the previous analysis without the b_g prior. Contours in the off-diagonal panels indicate the 68% and 95% confidence regions on the 2D plane, while histograms in the diagonal panels show the 1D posterior distributions of individual parameters, with thin dashed curves in the b_g and r_{gm} panels representing the Gaussian priors. The two sets of 1σ posterior constraints are listed in the top right.

Finally, in the bottom left panel of Figure 5, we successfully break the otherwise strong degeneracy between A and b_g with the help of the external prior, yielding a much better agreement with the *Planck* cosmology ($A=1\pm 0.007$; vertical dashed line). After marginalizing over the uncertainties in b_g and r_{gm} , we derive a stringent 1D constraint of $A=0.96\pm 0.07$, finding no tension with *Planck*.

5. CONCLUSION

In this letter, we develop a simple method based on the linear theory to assess the consistency between the clustering+lensing of BOSS LOWZ galaxies and the *Planck* cosmology. Focusing on scales $10 < R < 30 h^{-1}$ Mpc and assuming a fixed shape for the $P_{lin}(k)$, we can accurately model the clustering and lensing of galaxies using only three parameters, A , b_g , and r_{gm} , where $A=1$ in the *Planck* cosmology.

By examining the cross-correlation matrix of galaxy subsamples divided by stellar mass, we discover that the LOWZ galaxies with $\log M_* < 11.3$ are affected by some unknown observational systematics that lead to spurious correlations across large line-of-sight distances. We then build a clean LOWZ galaxy sample (C-LOWZ) by only including galaxies with $\log M_* > 11.3$. Applying our linear assessment model to the C-LOWZ sample, we obtain a constraint of $A=0.81^{+0.10}_{-0.09}$, which reproduces a 2σ tension with *Planck*.

However, there exists a strong degeneracy between our key parameter A and the nuisance parameter b_g . We develop a novel method of measuring b_g by combining the cluster-galaxy cross-correlation and cluster weak lensing using an overlapping sample of redMaPPer clusters. Intriguingly, despite the discrepancy between the biases inferred from clustering (2.00 ± 0.07) and lensing (1.63 ± 0.17) in *Planck*, both are consistent with our new cluster-based bias estimate (1.76 ± 0.22). Applying this independent bias measurement as a prior to our Bayesian analysis, we successfully break the degeneracy between A and b_g , and derive a stringent 1D posterior constraint of $A=0.96^{+0.07}_{-0.07}$, in good agreement with the *Planck* cosmology.

Our result suggests that the large-scale structure traced by the LOWZ galaxies at $z\sim 0.25$ is statistically consistent with *Planck*, while the clustering-lensing mismatch may be caused by some observational systematics (e.g., during the target selection). With the upcoming flux-limited galaxy sample at the same redshift from the Dark Energy Spectroscopic Instrument (Abareshi et al. 2022), we will acquire a clearer understanding of the clustering-lensing mismatch of the BOSS LOWZ sample, whether it be a tension of S_8 or b_g .

- 1 We thank Sukhdeep Singh, Zeyang Sun, and Jun Zhang
- 2 for helpful discussions. This work is supported by the Na-
- 3 tional Key Basic Research and Development Program of
- 4 China (No. 2018YFA0404504, 2022YFF0503403), the Na-
- 5 tional Science Foundation of China (12173024, 11890692,
- 6 11621303, 11973070, 11873038), the China Manned Space
- 7 Project (No. CMS-CSST-2021-A01, CMS-CSST-2021-A02,
- 8 CMS-CSST-2021-B01), and the “111” project of the Min-
- 9 istry of Education under grant No. B20019. Y.Z. acknowl-
- 10 edges the generous sponsorship from Yangyang Develop-
- 11 ment Fund, and thanks Cathy Huang for her hospitality dur-
- 12 ing the pandemic. H.S. acknowledges the Shanghai Commit-
- 13 tee of Science and Technology grant No.19ZR1466600 and
- 14 Key Research Program of Frontier Sciences, CAS, Grant No.
- 15 ZDBS-LY-7013.

REFERENCES

Abareshi, B., Aguilar, J., Ahlen, S., et al. 2022, *AJ*, 164, 207,
doi: 10.3847/1538-3881/ac882b

Aihara, H., Allende Prieto, C., An, D., et al. 2011, *ApJS*, 193, 29,
doi: 10.1088/0067-0049/193/2/29

- Alam, S., Albareti, F. D., Allende Prieto, C., et al. 2015, *ApJS*, 219, 12, doi: [10.1088/0067-0049/219/1/12](https://doi.org/10.1088/0067-0049/219/1/12)
- Alam, S., Aubert, M., Avila, S., et al. 2021, *PhRvD*, 103, 083533, doi: [10.1103/PhysRevD.103.083533](https://doi.org/10.1103/PhysRevD.103.083533)
- Amon, A., & Efstathiou, G. 2022, *MNRAS*, 516, 5355, doi: [10.1093/mnras/stac2429](https://doi.org/10.1093/mnras/stac2429)
- Amon, A., Gruen, D., Troxel, M. A., et al. 2022, *PhRvD*, 105, 023514, doi: [10.1103/PhysRevD.105.023514](https://doi.org/10.1103/PhysRevD.105.023514)
- Amon, A., Robertson, N. C., Miyatake, H., et al. 2023, *MNRAS*, 518, 477, doi: [10.1093/mnras/stac2938](https://doi.org/10.1093/mnras/stac2938)
- Asgari, M., Lin, C.-A., Joachimi, B., et al. 2021, *A&A*, 645, A104, doi: [10.1051/0004-6361/202039070](https://doi.org/10.1051/0004-6361/202039070)
- Baldauf, T., Smith, R. E., Seljak, U., & Mandelbaum, R. 2010, *PhRvD*, 81, 063531, doi: [10.1103/PhysRevD.81.063531](https://doi.org/10.1103/PhysRevD.81.063531)
- Beltz-Mohrmann, G. D., Szewciw, A. O., Berlind, A. A., & Sinha, M. 2022, arXiv e-prints, arXiv:2211.16105, doi: [10.48550/arXiv.2211.16105](https://doi.org/10.48550/arXiv.2211.16105)
- Cacciato, M., Lahav, O., van den Bosch, F. C., Hoekstra, H., & Dekel, A. 2012, *MNRAS*, 426, 566, doi: [10.1111/j.1365-2966.2012.21762.x](https://doi.org/10.1111/j.1365-2966.2012.21762.x)
- Chaves-Montero, J., Angulo, R. E., & Contreras, S. 2022, arXiv e-prints, arXiv:2211.01744. <https://arxiv.org/abs/2211.01744>
- Chen, Y.-M., Kauffmann, G., Tremonti, C. A., et al. 2012, *MNRAS*, 421, 314, doi: [10.1111/j.1365-2966.2011.20306.x](https://doi.org/10.1111/j.1365-2966.2011.20306.x)
- Contreras, S., Angulo, R. E., Chaves-Montero, J., White, S. D. M., & Aricò, G. 2022, arXiv e-prints, arXiv:2211.11745. <https://arxiv.org/abs/2211.11745>
- Dawson, K. S., Schlegel, D. J., Ahn, C. P., et al. 2013, *AJ*, 145, 10, doi: [10.1088/0004-6256/145/1/10](https://doi.org/10.1088/0004-6256/145/1/10)
- Dey, A., Schlegel, D. J., Lang, D., et al. 2019, *AJ*, 157, 168, doi: [10.3847/1538-3881/ab089d](https://doi.org/10.3847/1538-3881/ab089d)
- Eisenstein, D. J., Weinberg, D. H., Agol, E., et al. 2011, *AJ*, 142, 72, doi: [10.1088/0004-6256/142/3/72](https://doi.org/10.1088/0004-6256/142/3/72)
- Guo, H., Yang, X., & Lu, Y. 2018, *ApJ*, 858, 30, doi: [10.3847/1538-4357/aabc56](https://doi.org/10.3847/1538-4357/aabc56)
- Huterer, D. 2022, arXiv e-prints, arXiv:2212.05003, doi: [10.48550/arXiv.2212.05003](https://doi.org/10.48550/arXiv.2212.05003)
- Landy, S. D., & Szalay, A. S. 1993, *ApJ*, 412, 64, doi: [10.1086/172900](https://doi.org/10.1086/172900)
- Lange, J. U., Leauthaud, A., Singh, S., et al. 2021, *MNRAS*, 502, 2074, doi: [10.1093/mnras/stab189](https://doi.org/10.1093/mnras/stab189)
- Lange, J. U., Yang, X., Guo, H., Luo, W., & van den Bosch, F. C. 2019, *MNRAS*, 488, 5771, doi: [10.1093/mnras/stz2124](https://doi.org/10.1093/mnras/stz2124)
- Leauthaud, A., Saito, S., Hilbert, S., et al. 2017, *MNRAS*, 467, 3024, doi: [10.1093/mnras/stx258](https://doi.org/10.1093/mnras/stx258)
- Mandelbaum, R., Slosar, A., Baldauf, T., et al. 2013, *MNRAS*, 432, 1544, doi: [10.1093/mnras/stt572](https://doi.org/10.1093/mnras/stt572)
- More, S., Miyatake, H., Mandelbaum, R., et al. 2015, *ApJ*, 806, 2, doi: [10.1088/0004-637X/806/1/2](https://doi.org/10.1088/0004-637X/806/1/2)
- Planck Collaboration, Aghanim, N., Akrami, Y., et al. 2020, *A&A*, 641, A6, doi: [10.1051/0004-6361/201833910](https://doi.org/10.1051/0004-6361/201833910)
- Reid, B., Ho, S., Padmanabhan, N., et al. 2016, *MNRAS*, 455, 1553, doi: [10.1093/mnras/stv2382](https://doi.org/10.1093/mnras/stv2382)
- Reyes, R., Mandelbaum, R., Gunn, J. E., et al. 2012, *MNRAS*, 425, 2610, doi: [10.1111/j.1365-2966.2012.21472.x](https://doi.org/10.1111/j.1365-2966.2012.21472.x)
- Rykoff, E. S., Rozo, E., Busha, M. T., et al. 2014, *ApJ*, 785, 104, doi: [10.1088/0004-637X/785/2/104](https://doi.org/10.1088/0004-637X/785/2/104)
- Rykoff, E. S., Rozo, E., Hollowood, D., et al. 2016, *ApJS*, 224, 1, doi: [10.3847/0067-0049/224/1/1](https://doi.org/10.3847/0067-0049/224/1/1)
- Salcedo, A. N., Zu, Y., Zhang, Y., et al. 2022, *Science China Physics, Mechanics, and Astronomy*, 65, 109811, doi: [10.1007/s11433-022-1955-7](https://doi.org/10.1007/s11433-022-1955-7)
- Scolnic, D. M., Jones, D. O., Rest, A., et al. 2018, *ApJ*, 859, 101, doi: [10.3847/1538-4357/aab9bb](https://doi.org/10.3847/1538-4357/aab9bb)
- Secco, L. F., Samuroff, S., Krause, E., et al. 2022, *PhRvD*, 105, 023515, doi: [10.1103/PhysRevD.105.023515](https://doi.org/10.1103/PhysRevD.105.023515)
- Singh, S., Mandelbaum, R., Seljak, U., Rodríguez-Torres, S., & Slosar, A. 2020, *MNRAS*, 491, 51, doi: [10.1093/mnras/stz2922](https://doi.org/10.1093/mnras/stz2922)
- Takahashi, R., Sato, M., Nishimichi, T., Taruya, A., & Oguri, M. 2012, *ApJ*, 761, 152, doi: [10.1088/0004-637X/761/2/152](https://doi.org/10.1088/0004-637X/761/2/152)
- Tegmark, M., & Bromley, B. C. 1999, *ApJL*, 518, L69, doi: [10.1086/312068](https://doi.org/10.1086/312068)
- van den Bosch, F. C., More, S., Cacciato, M., Mo, H., & Yang, X. 2013, *MNRAS*, 430, 725, doi: [10.1093/mnras/sts006](https://doi.org/10.1093/mnras/sts006)
- Weinberg, D. H., Mortonson, M. J., Eisenstein, D. J., et al. 2013, *PhR*, 530, 87, doi: [10.1016/j.physrep.2013.05.001](https://doi.org/10.1016/j.physrep.2013.05.001)
- Wibking, B. D., Weinberg, D. H., Salcedo, A. N., et al. 2020, *MNRAS*, 492, 2872, doi: [10.1093/mnras/stz3423](https://doi.org/10.1093/mnras/stz3423)
- Yuan, S., Eisenstein, D. J., & Leauthaud, A. 2020, *MNRAS*, 493, 5551, doi: [10.1093/mnras/staa634](https://doi.org/10.1093/mnras/staa634)
- Zu, Y. 2020, arXiv e-prints, arXiv:2010.01143. <https://arxiv.org/abs/2010.01143>
- Zu, Y., & Mandelbaum, R. 2015, *MNRAS*, 454, 1161, doi: [10.1093/mnras/stv2062](https://doi.org/10.1093/mnras/stv2062)
- Zu, Y., Weinberg, D. H., Rozo, E., et al. 2014, *MNRAS*, 439, 1628, doi: [10.1093/mnras/stu033](https://doi.org/10.1093/mnras/stu033)
- Zu, Y., Shan, H., Zhang, J., et al. 2021, *MNRAS*, 505, 5117, doi: [10.1093/mnras/stab1712](https://doi.org/10.1093/mnras/stab1712)